Low-frequency inductive features in the electrochemical impedance spectra of mass-transport limited redox reactions

Debittree Choudhury, Rubul Das, Rajan Maurya, Geetanksha Gupta and Manoj Neergat*

Department of Energy Science and Engineering

Indian Institute of Technology Bombay, Powai, Mumbai, 400076, India

For any Faradaic reaction associated with the one-adsorbate system, the net rate of production/consumption of electrons (r_0) and the rate of production of the adsorbed species (r_1) are given by equations **S1** and **S2** [1, 2].

$$r_0 = \frac{i}{F} \tag{S1}$$

$$r_1 = \frac{q}{F}\left(\frac{d\theta}{dt}\right) \tag{S2}$$

Here, q is the charge required for complete coverage, and other symbols have their usual meanings. The faradaic admittance of the system, $\hat{Y}_f$, is therefore presented in equation **S3**.

$$\hat{Y}_f = \frac{\tilde{\imath}}{\tilde{\eta}} = A + \frac{B}{j\omega + C} \tag{S3}$$

The factors *A*, *B*, and *C* are given by equations **S4**, **S5**, and **S6**.

$$A = -F\left(\frac{\partial r_0}{\partial \eta}\right)_\theta \tag{S4}$$

$$B = -\frac{F^2}{q}\left(\frac{\partial r_0}{\partial \theta}\right)_\eta \left(\frac{\partial r_1}{\partial \eta}\right)_\theta \tag{S5}$$

$$C = -\frac{F}{q}\left(\frac{\partial r_1}{\partial \theta}\right)_\eta \tag{S6}$$

The behaviour of the system (capacitive/inductive) is decided by the factor B. Generally, if B > 0, the system behaviour is inductive, and the total impedance is given by equation **S7** [1, 2].

$$\hat{Z}_f = \frac{1}{\frac{1}{R_{ct}} + \frac{1}{j\omega L + R_0}} \tag{S7}$$

Here R_{ct} is the charge-transfer resistance, L is the inductance and R_0 serves as the inductive resistance, generally used to modify the phase delay between the voltage perturbation and the current response.

EI analysis of MOR

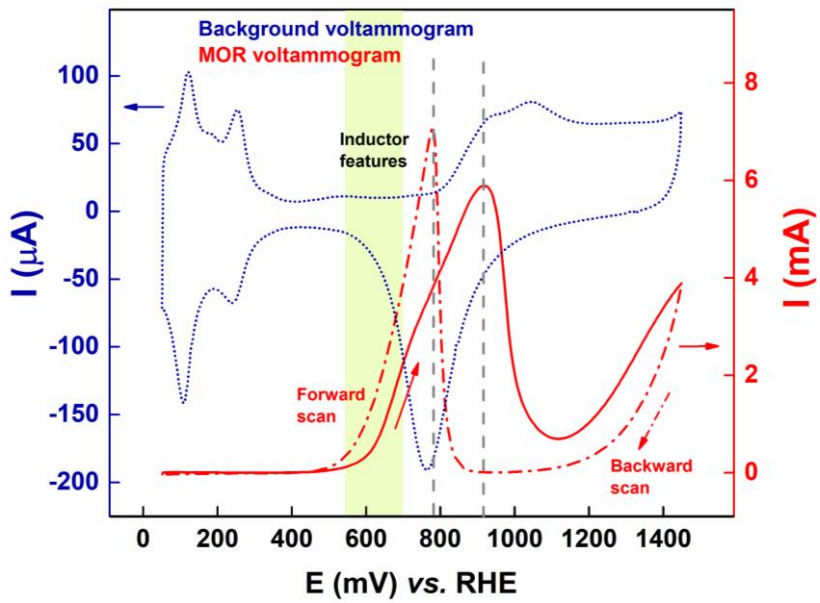

Figure S1 The voltammogram of methanol oxidation reaction (red trace) on Pt black in 0.25 M MeOH (0.5 M H_2SO_4). Solid and dotted lines correspond to forward and backward scan, respectively. The blue trace shows the background voltammogram of Pt black in methanol-free 0.5 M H_2SO_4.

Figure S1 presents the methanol oxidation voltammogram (red trace) in 0.5 M H_2SO_4 (0.25 M MeOH) and the background voltammogram (blue trace) in the supporting electrolyte on Pt black. The voltammogram of Pt shows typical polycrystalline features, *i.e.*, hydrogen underpotential deposition (H_{upd}) region (50–350 mV), double-layer region (400–600 mV), and oxide formation/reduction region (600–1100 mV). In the H_{upd} region, H atoms adsorb/desorb on Pt surface, featuring sharp H_{upd} peaks at 125 mV and 270 mV corresponding to Pt (110) and Pt (100) step sites, respectively [3, 4]. In the double-layer region, no charge-transfer occurs. From 600 mV onwards, surface oxidation starts and the oxides get reduced in the reverse scan.

The first peak appears at ~900 mV in the MOR voltammogram, suggesting the increasing methanol oxidation current with overpotential. The details of the reactions up to potential ~900 mV in the forward scan of the MOR voltammogram are explained in the main manuscript. The decrease in the oxidation current at potential above ~900 mV suggests extensive surface oxidation that inhibits the methanol oxidation. This is evident from the background CV as well (blue trace). At higher potentials, methanol present in the electrolyte

starts oxidizing again at ~1200 mV; here the oxygen source is assumed to be the oxide itself [5].

In the backward scan, once the surface oxide starts to reduce at potential down to ~850 mV (see the background CV in Figure S1), pristine Pt surface is obtained and the sites are available for methanol oxidation. Here, the simultaneous methanol dehydrogenation and oxidative removal of CO_{ad} causes a sharp increase in the current. But with decreasing potential in the reverse scan, the current due to methanol dehydrogenation and the OH_{ad} formation decreases exponentially. The oxidation peak of methanol appears at comparatively lower potential (~800 mV) in the reverse scan because the surface is free from any competing oxygenated species for adsorption, and a hysteresis is observed.

$$CH_3OH \rightarrow CO_{ad} + 4H^+ + 4e^- \quad \textbf{(S8)}$$

$$H_2O \rightarrow OH_{ad} + H^+ + e^- \quad \textbf{(S9)}$$

$$CO_{ad} + OH_{ad} \rightarrow CO_2 + H^+ + e^- \quad \textbf{(S10)}$$

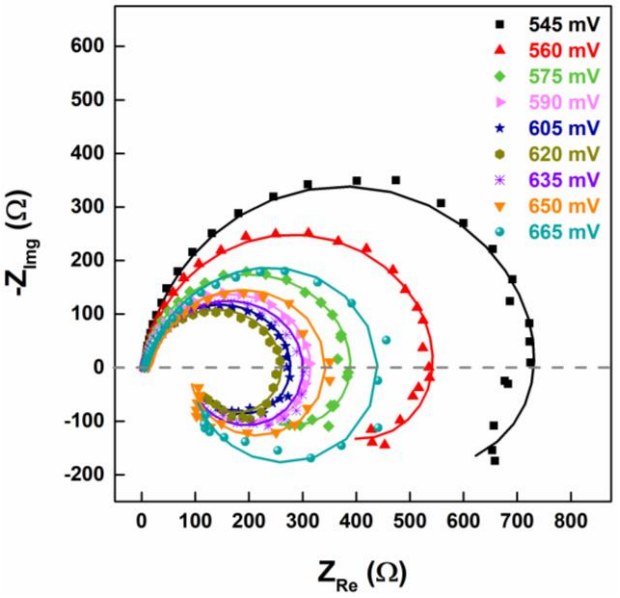

Figure S2 Nyquist plots of MOR on Pt black in argon-saturated 0.25 M MeOH (in 0.5 M H_2SO_4 electrolyte) at a potential interval of 15 mV.

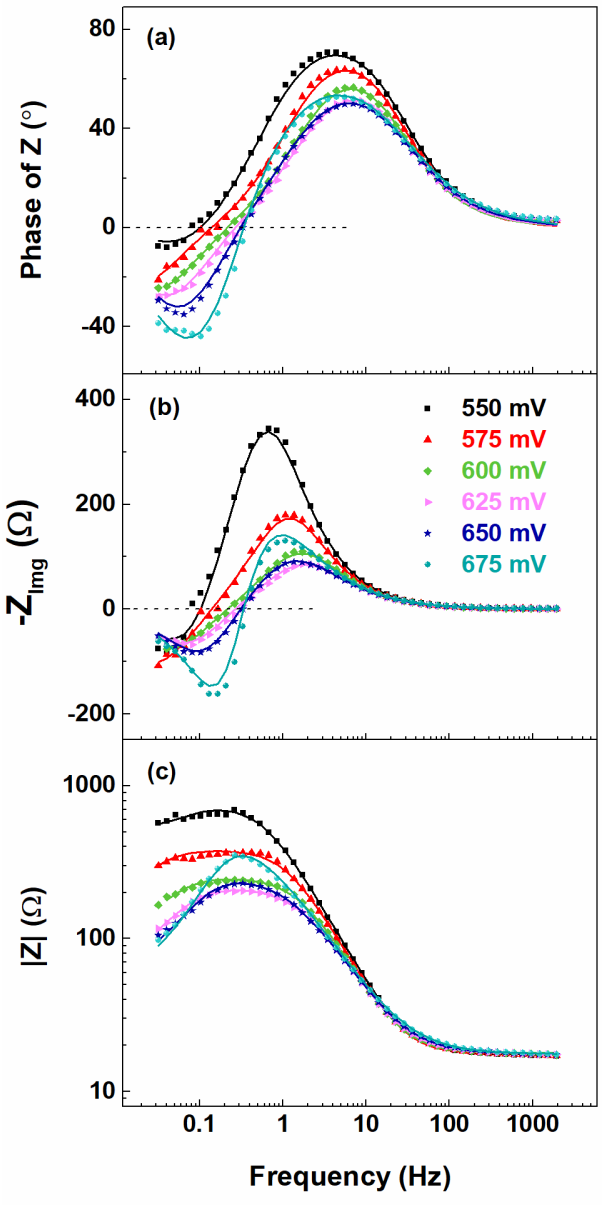

Figure S3 (a) Phase, (b) imaginary, and (c) magnitude Bode plots of MOR on Pt black in 0.25 M MeOH (0.5 M H_2SO_4).

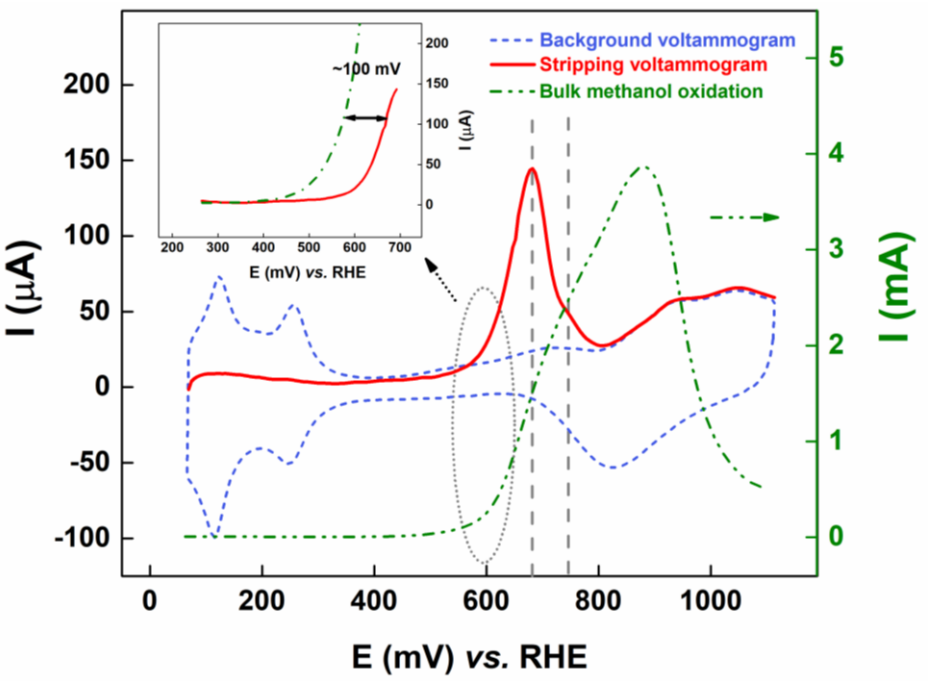

Figure S4 Methanol stripping voltammogram (red trace) on Pt black in a 0.5 M H_2SO_4 solution. The blue trace shows the background voltammogram. The green trace shows the bulk methanol oxidation voltammogram in the forward scan.

During the stripping experiment, a sharp oxidation peak is observed at ~700 mV in the first forward scan. In the second forward scan, the CO oxidation peak does not appear, and clean H_{upd} is obtained, indicating complete stripping of adsorbed CO (CO_{ad}) during the first forward scan [6, 7]. Both scans are presented in the **Figure S4**.

The onset of methanol dehydrogenation starts at ~450 mV, which is ~100 mV down to the onset potential of CO oxidation during the stripping (see inset to Figure S4). The sharp oxidation peak in the stripping voltammogram (red trace) (at ~700 mV) nearly matches with the shoulder peak in the bulk methanol oxidation CV in a methanol-containing electrolyte (green trace). Thereafter, the current increases at potential above ~700 mV due to the oxidative removal of CO_{ad} by the OH_{ad} during MOR. The shoulder peak at ~750 mV in the stripping voltammogram is possibly due to the oxidation of CO at different orientation of Pt [8]. From ~900 mV onwards, the current starts decreasing in the MOR voltammogram due to high surface coverage by the oxygenated species, as evident from the background voltammogram.

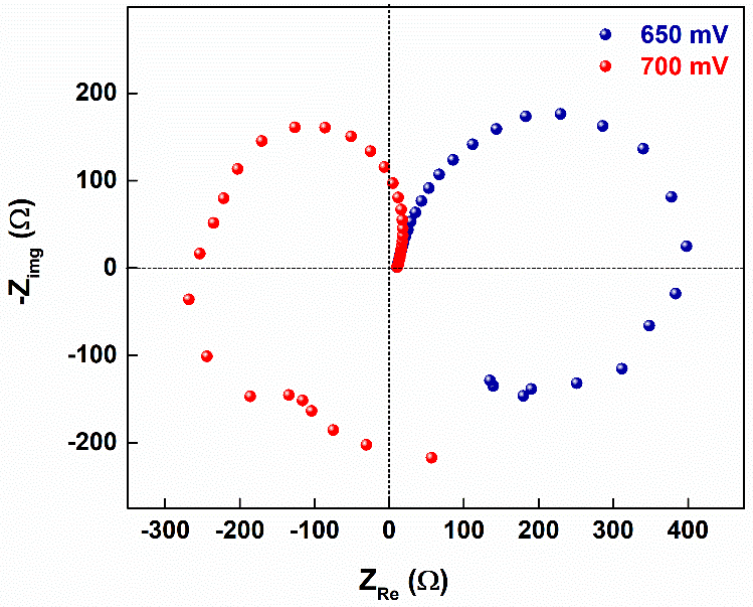

Figure S5 Nyquist plots of MOR in two different potential regions. Red trace features the change in *rds* from CO oxidation to excessive formation of surface OH_{ad}.

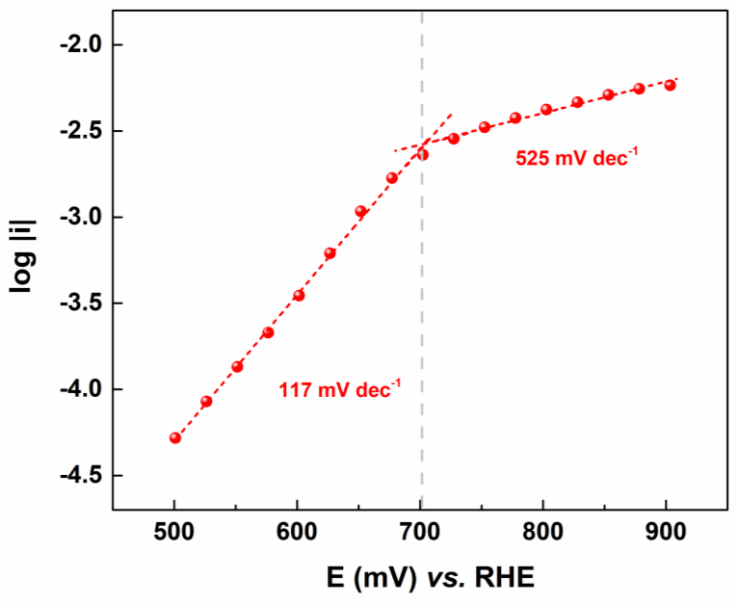

Figure S6 Tafel plot of MOR recorded in 0.25 M MeOH (0.5 M H_2SO_4).

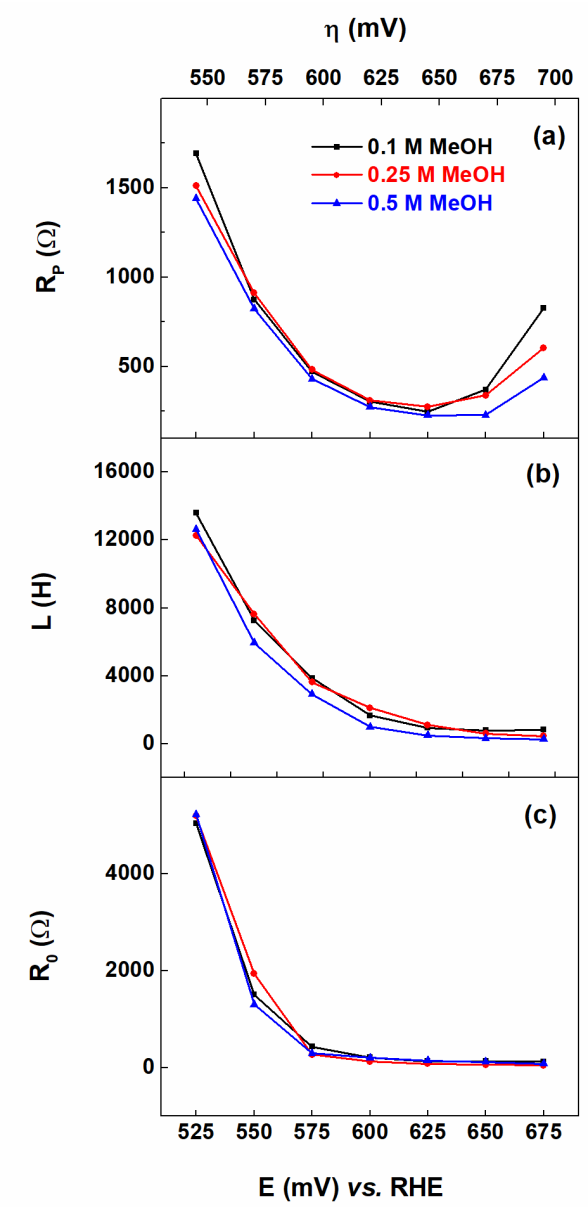

Figure S7 Trends in (a) R_P, (b) L, and (c) R_0 of MOR at different MeOH concentrations on Pt black.

Table S1 Trend in the values of R_P, L and R_0 with potential for methanol oxidation reaction on Pt black (loading: 125 μg cm^{-2}) in 0.5 M H_2SO_4 (0.25 M MeOH)

E (mV)	R_P (Ω)	L (H)	R_0 (Ω)
525	1358±44	15583±1840	4104±440
550	683±31	7707±1552	1464±142
575	384±10	2786±204	365±19
600	249±11	1237±39	151±12
625	210±9	653±23	101±7
650	259±63	431±17	83±8
675	413±46	332±14	66±7

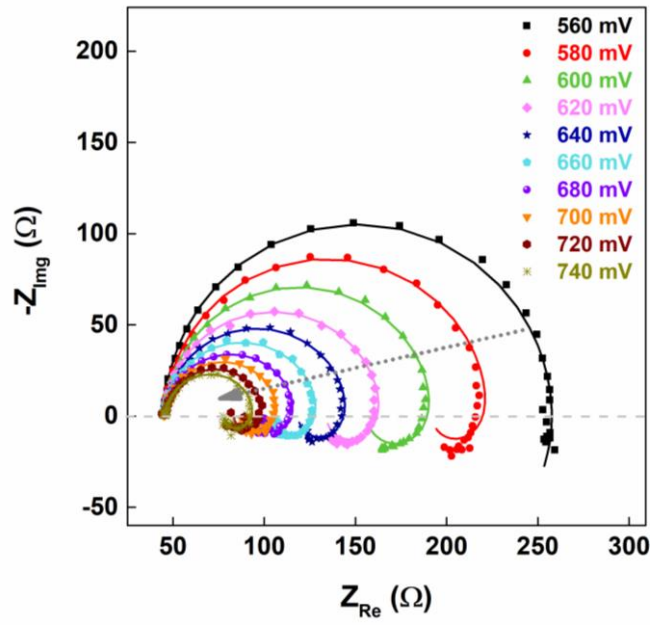

Figure S8 Nyquist plots of MOR on Pt black in argon-saturated 0.25 M MeOH (in 0.1 M NaOH electrolyte).

The mechanism of MOR in the alkaline medium is the following [9].

$$CH_3OH + 3OH^- \leftrightarrow HCO_{ad} + 3H_2O + 3e^- \quad \textbf{(S11)}$$

$$OH^- \leftrightarrow OH_{ad} + e^- \quad \textbf{(S12)}$$

$$HCO_{ad} + OH_{ad} \rightarrow HCOOH \quad \textbf{(S13)}$$

$$HCOOH + OH^- \rightarrow HCOO^- + H_2O \quad \textbf{(S14)}$$

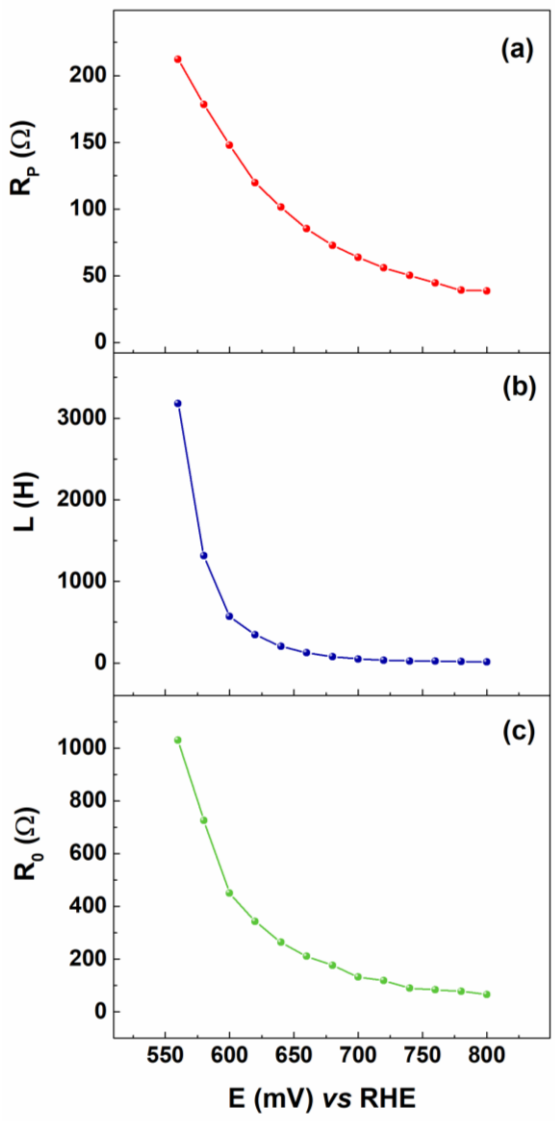

Figure S9 Trend in (a) R_p, (b) L, and (c) R_0 values with potential for MOR on Pt black in 0.25 M MeOH (0.1 M NaOH) electrolyte.

EI analysis of ORR

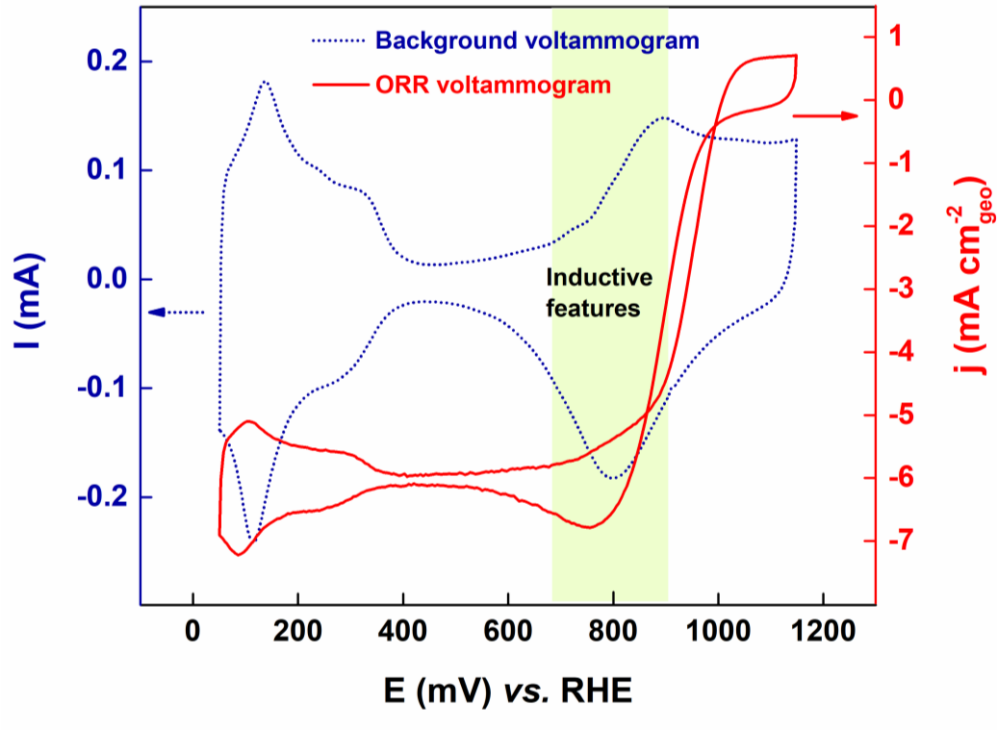

Figure S10 Background voltammogram (blue trace) and ORR polarization curve (red trace) of Pt black (loading: 125 µg cm^{-2}) in argon-saturated and oxygen-saturated 0.1 M $HClO_4$, respectively.

Figure S10 presents the ORR voltammogram on Pt black (red trace) in oxygen-saturated 0.1 M $HClO_4$ along with the corresponding background voltammogram (blue trace) in argon-saturated 0.1 M $HClO_4$. The voltammogram shows Pt polycrystalline features as discussed earlier. From 600 mV onwards, various surface oxygenated species start forming [10, 11].

$$O_2 + Pt + Pt\text{–}H_2O \rightleftarrows PtOH_{ad} + Pt\text{–}O\text{–}O\text{–}H \quad \textbf{(S15)}$$

$$PtOH_{ad} + H^+ + e^- \rightleftarrows Pt + H_2O \quad \textbf{(S16)}$$

$$Pt\text{–}O\text{–}O\text{–}H + Pt(H_2O) \rightarrow Pt(OH)_2 + PtOH_{ad} \quad \textbf{(S17)}$$

The red trace in Figure S10 presents the ORR voltammogram on Pt black electrode in oxygen-saturated 0.1 M $HClO_4$. A hysteresis between the forward and backward scans is observed in the ORR voltammogram. During the forward scan (positive scan direction),

pristine Pt surface is available for ORR. While in the backward scan (negative scan direction), the surface oxide formed at higher potentials blocks the active sites, and hence ORR occurs on Pt surface partially covered with oxygenated species, which eventually lowers the kinetic current and causes a hysteresis. The ORR curve has three regions, that is, kinetic limited region (1050–950 mV), mixed kinetic diffusion-controlled region (900–800 mV) and mass-transfer limited region (800 mV onwards).

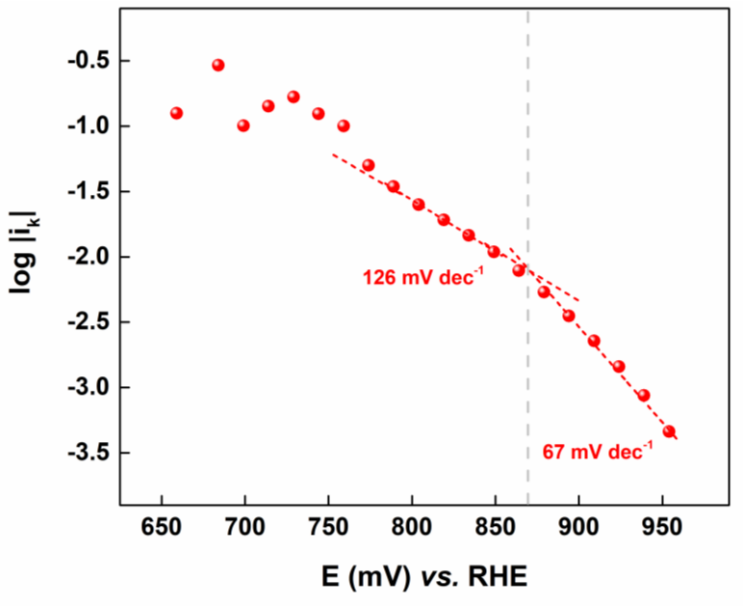

Figure S11 Tafel slope of ORR in oxygen-saturated 0.1 M $HClO_4$.

The Tafel plot of ORR is presented as log i_k *vs.* E in **Figure S11**. The total current is corrected for the limiting current using Koutecky-Levich equation as follows [12].

$$\frac{1}{i} = \frac{1}{i_k} + \frac{1}{i_l} \qquad \textbf{(S18)}$$

Here, i is the total current, i_k the kinetic current, and i_l is the limiting current.

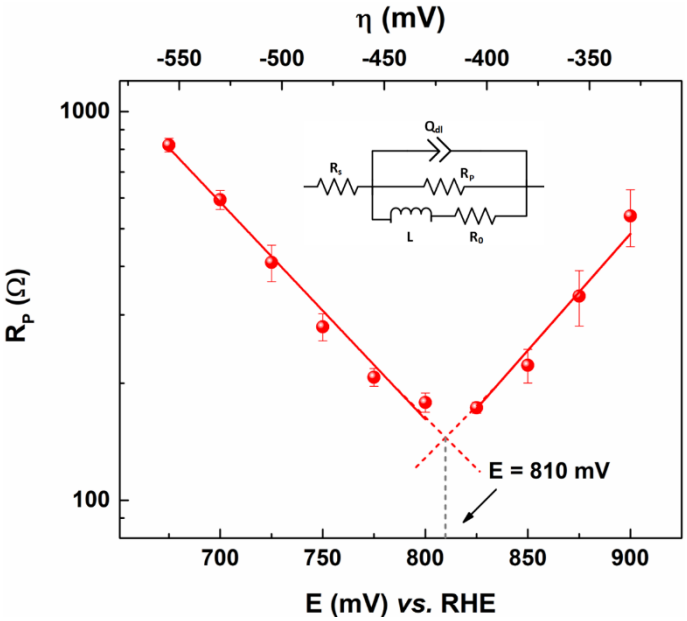

Figure S12 Trend in R_P values for ORR on Pt black in 0.1 M $HClO_4$. Inset shows the equivalent circuit used to fit the experimental data.

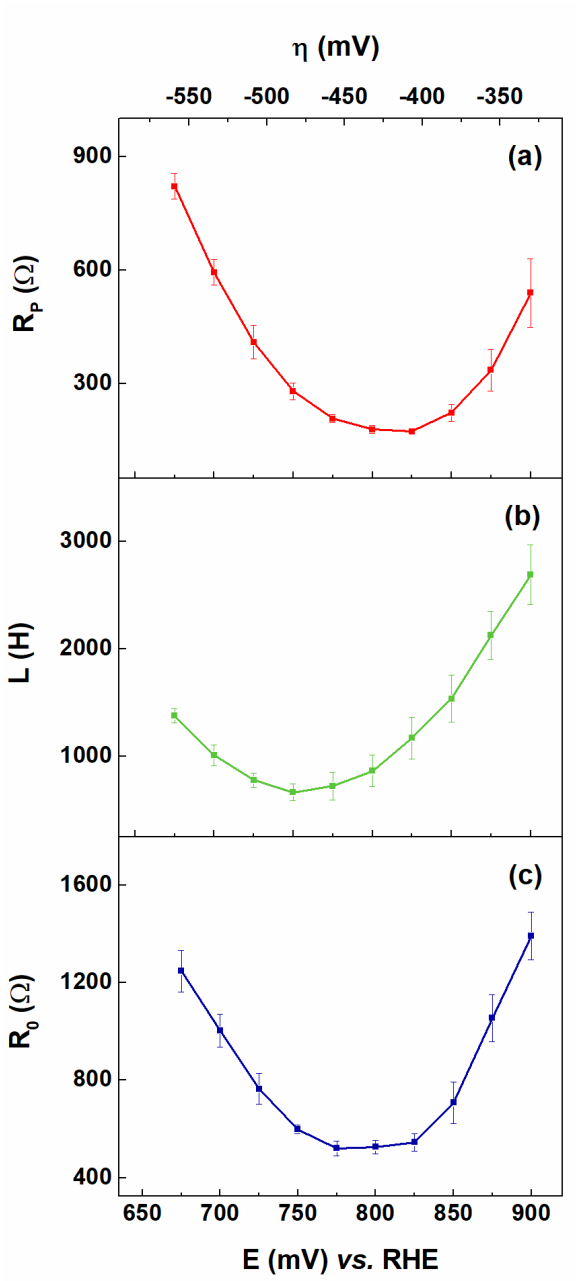

Figure S13 The trend in (a) R_P, (b) L, and (c) R_0 values as functions of potential for complete ORR region.

Table S2 Trend in the values of R_P, L, and R_0 with potential for ORR on Pt black (loading: 125 μg cm^{-2}) in 0.1 M $HClO_4$

E (mV)	R_P (Ω)	L (H)	R_0 (Ω)
900	540±80	2691±280	1392±97
875	335±52	2125±226	1054±96
850	223±22	1537±217	708±84
825	173±5	1171±194	545±36
800	178±10	863±147	526±48
775	207±10	721±128	520±50
750	280±22	663±80	597±17
725	409±40	779±66	764±63
700	594±32	1011±96	1004±68
675	821±33	1377±66	1248±85

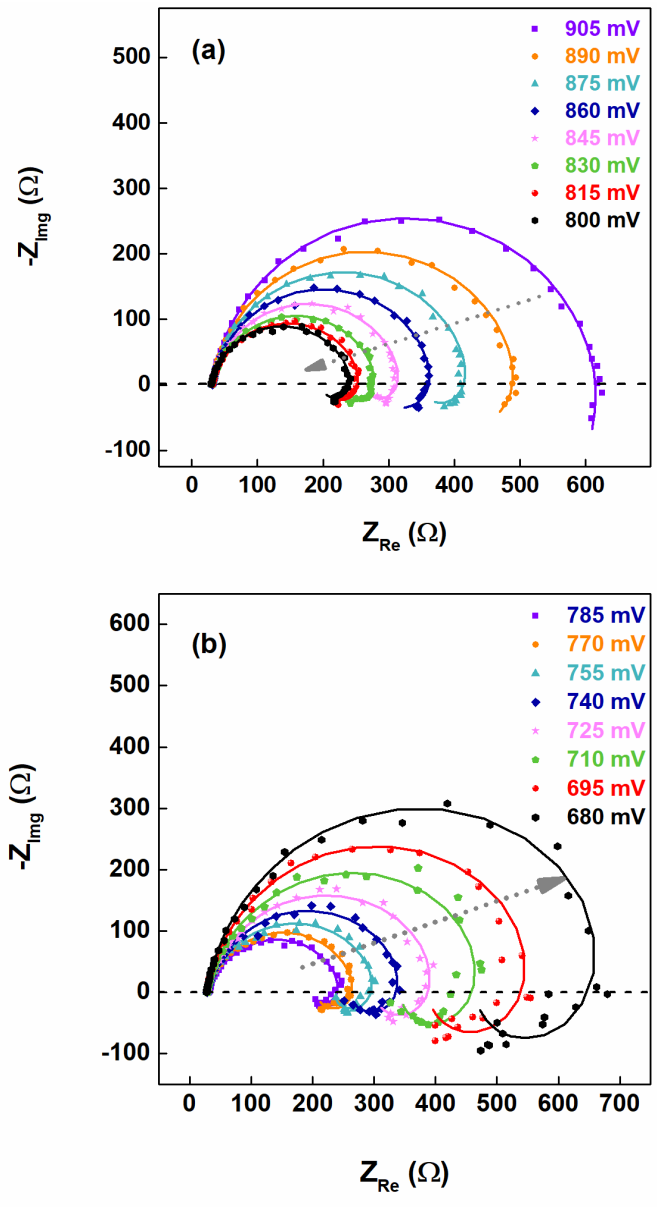

Figure S14 Nyquist plots of ORR in oxygen-saturated 0.1 M $HClO_4$ in the (a) mixed kinetic-diffusion-controlled, and (b) mass-transport limited regions at a potential interval of 15 mV.

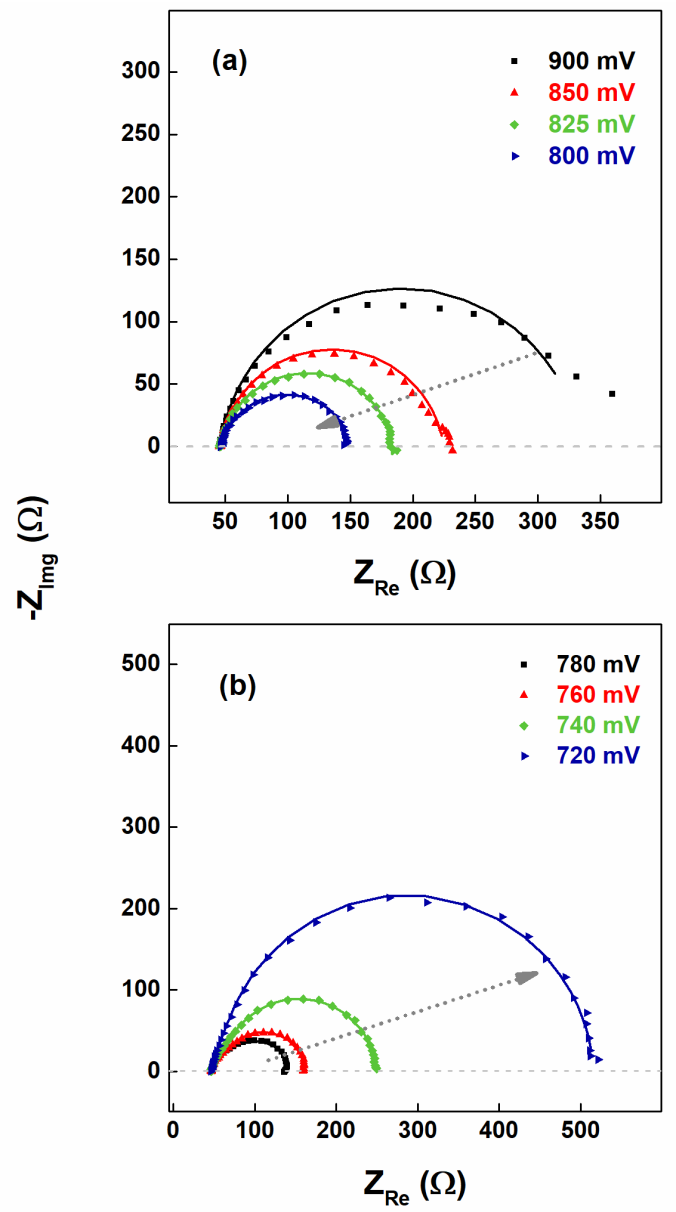

Figure S15 Nyquist plots of ORR on Pt black in oxygen-saturated 0.1 M NaOH in the (a) mixed kinetic-diffusion-controlled, and (b) mass-transport limited regions.

The mechanism of ORR in alkaline medium is the following [13].

$$O_2 + e^- \rightleftarrows (O_2^-)_{ad} \quad \textbf{(S19)}$$

$$(O_2^-)_{ad} + H_2O \rightarrow (HO_2)_{ad}^- + OH \quad \textbf{(S20)}$$

$$OH + e^- \rightarrow OH^- \quad \textbf{(S21)}$$

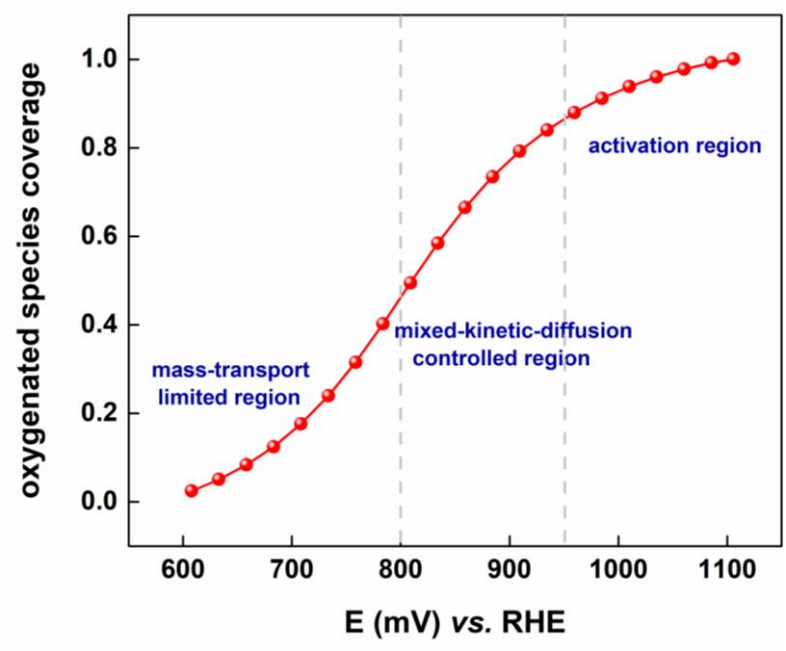

Figure S16 Adsorption isotherm at room temperature (298 K) for oxygen reduction on Pt black in oxygen-saturated 0.1 M $HClO_4$.

Figure S16 presents the adsorption isotherm, obtained from the background voltammogram of Pt black in 0.1 M $HClO_4$ (Figure S10). The charge from the oxide reduction peak is integrated from 1100 mV to 600 mV to obtain the change in oxygenated species coverage with potential in the experimental potential range of ORR. The oxygenated species coverage is taken as 1 at 1100 mV, the starting potential of ORR in this work and the relative decrease in coverage with potential is calculated from the charge integrated at each potential.

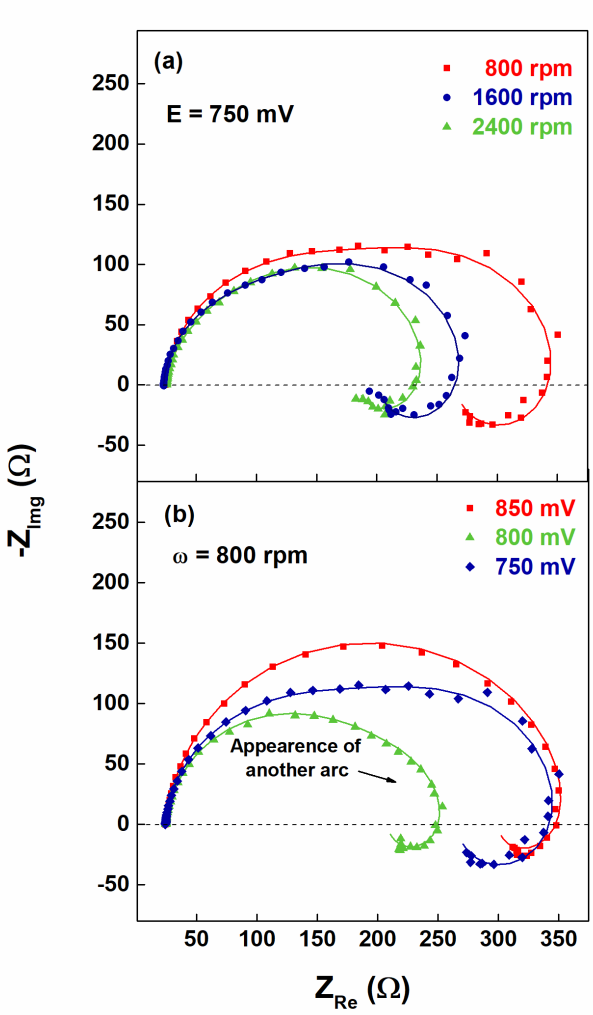

Figure S17 Nyquist plots of ORR on Pt black in oxygen-saturated 0.1 M $HClO_4$ at (a) a constant potential of 750 mV, and at rotation rate from 800 to 2400 rpm, and (b) constant rotation of 800 rpm, and varying the potential in the mass-transport limited region.

Table S3 Trend in the values of *L* and R_0 with rotation rate for ORR on Pt black (loading: 125 μg cm^{-2}) in 0.1 M $HClO_4$ at 750 mV

ω (rpm)	L (H)	R_0 (Ω)
800	1212	851.3
1600	431.2	582.9
2400	349.3	528.2

Table S4 Trend in the values of *L* and R_0 with rotation rate for ORR on Pt black (loading: 125 μg cm^{-2}) in 0.1 M $HClO_4$ at a rotation rate of 800 rpm

E (mV)	L (H)	R_0 (Ω)
850	1560	1325
800	1028	844
750	1212	852

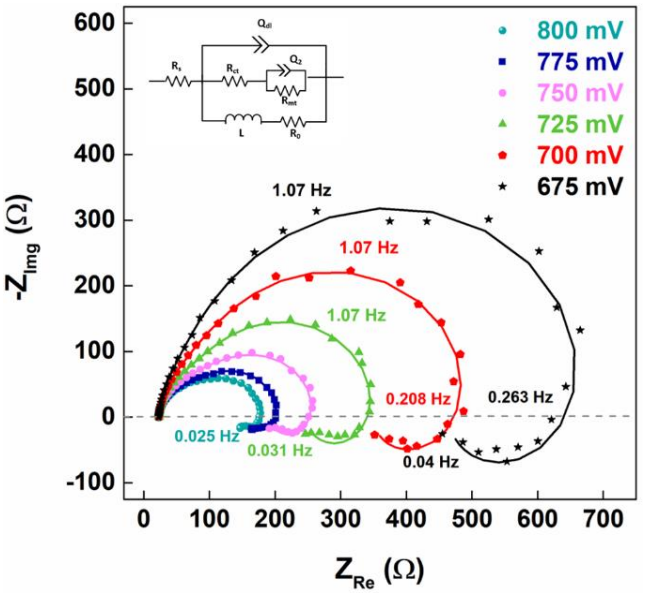

Figure S18 Nyquist plots for ORR on Pt black in 0.1 M $HClO_4$ in the mass-transport limited region. Inset shows the equivalent circuit used to fit the experimental data.

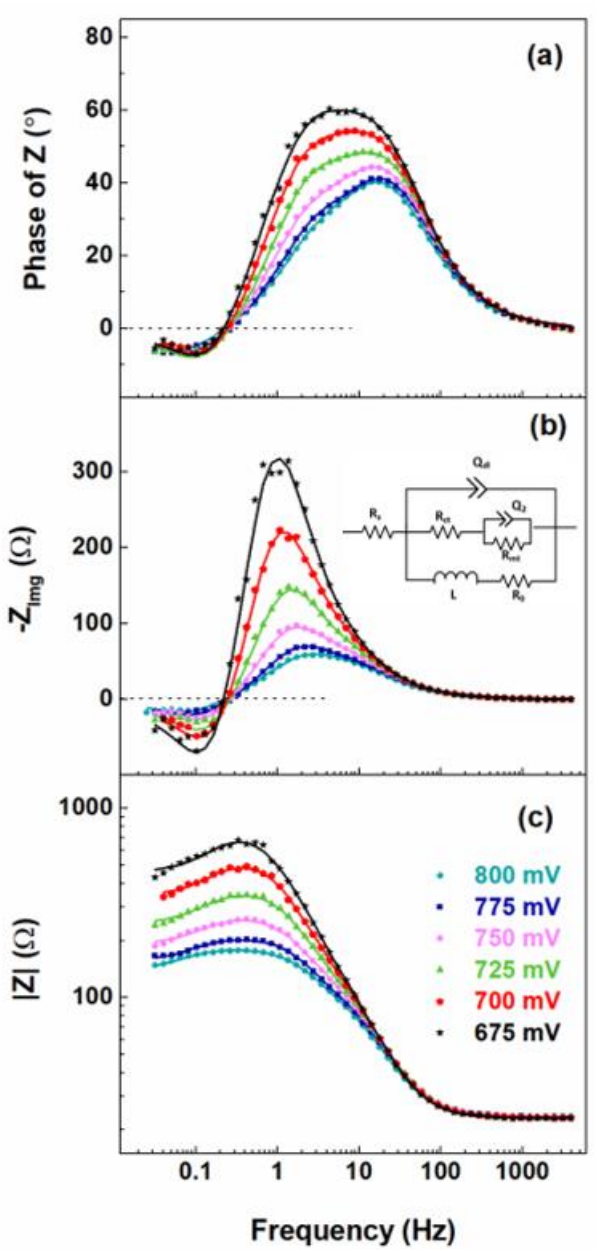

Figure S19 Phase (a), imaginary (b), and magnitude (c) Bode plots of ORR in oxygen-saturated 0.1 M $HClO_4$ in the mass-transport limited region. Inset shows the equivalent circuit used to fit the experimental data.

Table S5 Trend in the values of R_{ct}, R_{mt}, L, and R_0 with potential for ORR on Pt black (loading: 125 μg cm^{-2}) in oxygen-saturated 0.1 M $HClO_4$. The data is fitted with the circuit 2 presented in main manuscript.

E (mV)	R_{ct} (Ω)	R_{mt} (Ω)	L (H)	R_0 (Ω)
800	131±12	47±3	901±140	515±26
775	134±13	68±3	763±45	536±26
750	150±11	119±5	851±32	619±33
725	188±22	209±18	1010±37	811±32
700	238±23	348±70	1280±108	1007±64
675	314±27	489±40	1598±67	1415±88

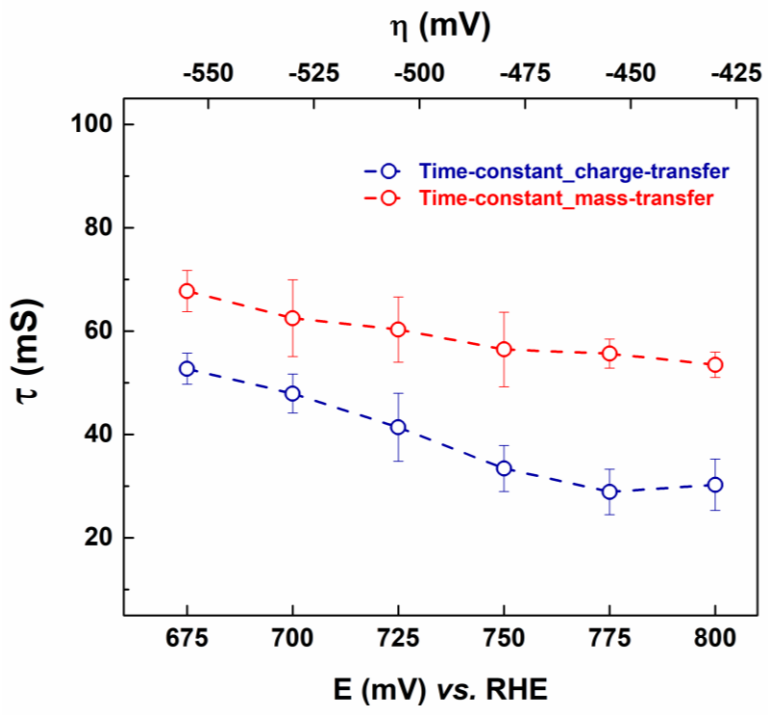

Figure S20 The variation of the time-constants associated to charge-transfer and mass-transfer processes in the mass-transport limited region as function of potential.

$$\tau = R \times C \qquad \textbf{(S22)}$$

Table S6 Parameters obtained by fitting the EIS pattern of ORR recorded at 800 mV (ω = 1600 rpm) in 0.1 M $HClO_4$ solution. The EC presented in Figure 1 (Circuit 1) is used for fitting the data.

Parameter	**Obtained fitting value**	**Relative standard error (%)**	**χ^2 value**	**Relative error of the measured impedance**
R_s	22.7	1.00	0.00166	3.036
R_P	254.6	2.18		
Q_1 (S. sec$^{\varphi}$)	0.0002549	4.41		
Φ_1	0.8195	1.16		
L	860.6	11.00		
R_0	509.8	7.18		

Table S7 Parameters obtained by fitting the EIS pattern of ORR recorded at 800 mV (ω = 1600 rpm) in 0.1 M $HClO_4$ solution. The EC presented in Figure 2 (Circuit 2) is used for fitting the data.

Parameter	**Obtained fitting value**	**Relative standard error (%)**	**χ^2 value**	**Relative error of the measured impedance**
R_s	23.28	0.44	0.000215	1.566
R_{ct}	135	4.41		
Q_1 (S. sec$^{\varphi}$)	0.0002327	4.48		
Φ_1	0.93	1.17		
R_{mt}	111.2	6.26		
Q_2 (S. sec$^{\varphi}$)	0.0006361	5.36		
Φ_2	0.99	4.68		
L	893.7	7.30		
R_0	578.5	3.48		

The EIS pattern recorded at 800 mV (onset of mass-transport) is fitted with both the circuits presented in Figures 1 and 2. The F-test help justifying the use of the latter circuit over the former statistically.

Number of degrees of freedom $v = 2N - m$

N is the number of frequencies ($2N$ is used because $2N$ measured impedance values; N real and N imaginary), and m is the number of adjustable parameters in the model.

$N = 55$, $m = 6$

k is the number of parameters added in the new model.

$k = 3$, $\alpha = 0.05$

$F(\alpha, k, 2N - m - k) = 2.6928$ (calculated in excel using F.INV.RT)

$$F_{exp} = \frac{\frac{S_1 - S_2}{(2N - m) - (2N - m - k)}}{\frac{S_2}{(2N - m - k)}} = \frac{S_1 - S_2}{S_2} \times \frac{(2N - m - k)}{k}$$

$S_1 = 3.036$, $S_2 = 1.566$

Therefore, $F_{exp} = 48.36$

$F_{exp} > F(\alpha, k, 2N - m - k)$

Hence, the circuit containing the mass-transfer element (Circuit 2) is better acceptable.

References

1. D. A. Harrington and B. E. Conway, *Electrochim. Acta*, 1987, **32**, 1703–1712.
2. A. Lasia, *Electrochemical Impedance Spectroscopy and its Applications*; Springer: New York, 2014.
3. R. Devivaraprasad, R Ramesh, N. Naresh, T. Kar, R. K. Singh, and M. Neergat, *Langmuir*, 2014, **30**, 8995–9006.
4. J. Solla-Gullon, F. J. Vidal-Iglesias, A. Lopez-Cudero, E. Garnier, J. M. Feliu, and A. Aldaz, *Phys. Chem. Chem. Phys.*, 2008, **10**, 3689–3698.
5. F. Seland, R. Tunold and D. A. Harrington, *Electrochim. Acta*, 2006, **51**, 3827–3840.
6. Y. Zhou, Y. Kuang, G. Hu, X. Wang, and L. Feng, *Mater. Today Phys*., 2022, **27**, 100831.
7. Y. Zhou, Q. Wang, X. Tian, and L. Feng, *Nano Res*., 2022, **15**, 8936−8945.
8. A. Cuesta, A. Couto, A. Rincon, M.C. P´rez, A. Lopez-Cudero, C. Gutierrez, *J. Electroanal. Chem.*, 2006, **586**, 184–195.
9. A. V. Tripkovic, K. D. Popovic, J. D. Lovic, V. M. Jovanovic, A. Kowal, *J. Electroanal. Chem.*, 2004, **572**, 119–128.
10. A. Damjanovic and V. Brusic, *Electrochim. Acta*, 1967, **12**, 615–628.
11. D. B. Sepa, M. V. Voinovic and A. Damjanovic, *Electrochim. Acta*, 1981, **26**, 781–793.
12. A. Bard and L. Faulkner, *Electrochemical Methods: Fundamentals and Applications*; pp 341, chapter 9, John Wiley and Sons: New York, 2001.
13. A. Damjanovic, M. A. Genshaw, and J. O'M. Bockris, *J. Electrochem. Soc*., 1967, **114**, 1107–1112.